Journal of Materials Chemistry A

COMMUNICATION

View Article Online
View Journal | View Issue

Cite this: J. Mater. Chem. A, 2017, 5, 19607

Received 20th June 2017
Accepted 4th September 2017

DOI: 10.1039/c7ta05392d

rsc.li/materials-a

Novel barium titanate based capacitors with high energy density and fast discharge performance†

Wen-Bo Li,[a] Di Zhou, *[ac] Li-Xia Pang,[bc] Ran Xu[a] and Huan-Huan Guo[a]

Recently, dielectric capacitors have attracted much attention due to their high power density based on fast charge–discharge capability. However, their energy storage applications are limited by their low discharge energy densities. In this work, we designed novel lead-free relaxor-ferroelectric $0.88BaTiO_3$–$0.12Bi(Li_{0.5}Nb_{0.5})O_3$ (0.88BT–0.12BLN) ceramics with high breakdown strength and high discharge energy density. The 0.88BT–0.12BLN ceramics were prepared by a conventional solid state reaction method. Optimal energy storage properties were obtained in 0.88BT–0.12BLN ceramics sintered at 1220 °C with an impressive discharge energy density of 2.032 J cm^{-3} and a charge–discharge efficiency of beyond 88% at 270 kV cm^{-1}. The energy storage properties of the 0.88BT–0.12BLN also displayed good thermal stability from 20 to 120 °C at an electric field of 150 kV cm^{-1}. Moreover, the discharge speed behavior was investigated by using pulsed current. The pulsed discharge current waveforms showed that all the samples have fast discharge times (less than 0.5 μs) under different electric fields. This work significantly increases the intrinsic breakdown strength and discharge energy density of $BaTiO_3$-based materials with high charge–discharge efficiency for high power energy storage devices.

Nowadays dielectric capacitors have attracted much attention due to their high power density based on ultrafast charge–discharge capability (<1 μs).[1–5] However, their energy storage applications are limited by their low discharge energy densities. In modern electronics and electrical power systems, capacitors with high energy density can reduce the volume, weight, and cost of electronic and energy storage devices.[6–10] So, the low breakdown strength and discharge energy density of capacitors still limit their application in high-voltage equipment and compact electronic devices.[11–13] It is important to search for new materials with high breakdown strength and discharge energy density to meet the increasing demands for more compact electronic and energy storage devices.

For dielectric capacitors, high maximum polarization (P_{max}), low remnant polarization (P_r) and high breakdown strength are desired for achieving high discharge energy density and energy conversion efficiency (%). In general, anti-ferroelectric (AFE) and ferroelectric (FE) ceramic materials are strong candidates. As for antiferroelectric and ferroelectric ceramics, it is well known that the energy storage density (W) is determined by the dielectric constant and the breakdown strength:[14]

$$W = \int_0^{P_{max}} E\mathrm{d}P \quad (1)$$

$$W_{dis} = \int_{P_r}^{P_{max}} E\mathrm{d}P \quad (2)$$

$$\eta = \frac{W_{rec}}{W} \times 100\% \quad (3)$$

where W, W_{dis}, E, P_r, P_{max} and η are the charge energy density, the discharge energy density, the electric field, the remnant polarization, the maximum polarization and the charge–discharge energy efficiency, respectively. AFE and FE ceramics are promising for high-power energy storage applications because of their large dielectric constant. However, the interior defect of pores during the sintering route and their high remnant polarization make AFE and FE ceramics exhibit low breakdown strength (<200 kV cm^{-1}) and discharge energy storage density (<2 J cm^{-3}).[15–17]

In recent years, many efforts have been focused on improving the energy storage properties of AFE and FE. According to eqn (2), there are two possible routes to improve the discharge energy density of AFE and FE ceramics for energy storage applications: one is to enhance the breakdown strength.

[a]Electronic Materials Research Laboratory, Key Laboratory of the Ministry of Education, International Center for Dielectric Research, Xi'an Jiaotong University, Xi'an 710049, Shaanxi, China. E-mail: zhoudi1220@gmail.com; Fax: +86-29-82668679; Tel: +86-29-82668679

[b]Micro-optoelectronic Systems Laboratories, Xi'an Technological University, Xi'an 710032, Shaanxi, China

[c]Department of Materials Science and Engineering, University of Sheffield, S1 3JD, UK

† Electronic supplementary information (ESI) available. See DOI: 10.1039/c7ta05392d

Another is to increase the limit of integration by enlarging the difference between the P_r and P_{max}. For example, AFE ceramic $(Pb_{0.88}La_{0.08})(Zr_{0.91}Ti_{0.09})O_3$ possesses a W_{dis} of 3.04 J cm^{-3}, a η of 92% under near breakdown strength (170 kV cm^{-1}).[18] Then AFE ceramic $(Pb_{0.97-x}Sr_xLa_{0.02})(Zr_{0.75}Sn_{0.195}Ti_{0.055})O_3$ has a higher energy density (5.56 J cm^{-3}) because of the higher applied electric field (350 kV cm^{-1}).[19] $BaTiO_3$ is an important lead-free FE material and a widely used capacitor material. As for $BaTiO_3$-based FE ceramics, some oxides with extra high breakdown strength are used as additives to enhance the breakdown strength of $BaTiO_3$-based FE ceramics, such as Al_2O_3, SiO_2, MgO and so on.[20–22] For example, $BaTiO_3$ ceramics coated with powders of Al_2O_3 and SiO_2 with an enhanced energy storage density of 0.725 J cm^{-3} with $\eta \sim 80\%$ had been prepared by Liu *et al.*[20] Huang *et al.*[21] obtained the BST-MgO composite by spark plasma sintering with the W_{dis} about 1.5 J cm^{-3} and $\eta \sim$ 88.5%. While previous work mainly focused on increasing the breakdown strength values to obtain larger energy storage density, less attention was paid to the technique of enlarging the difference between P_{max} and P_r values. A recent study has shown that relaxor ferroelectrics exhibit high energy density with a large difference between the P_{max} and P_r values (high P_{max}, lower P_r and slim hysteresis loop). For example, Shen *et al.* found that $0.91BaTiO_3$–$0.09BiYbO_3$ ceramics exhibited an energy storage density of 0.71 J cm^{-3} at 93 kV cm^{-1}.[23] Then a series of relaxor ferroelectric $BaTiO_3$–$Bi(M_{2/3}Nb_{1/3})O_3$ and $BaTiO_3$–$Bi(M_{1/2}Ti_{1/2})O_3$ (M = Mg and Zn) ceramics were studied and the energy storage density varied between 0.7 and 1.81 J cm^{-3}.[24–28] As a promising candidate system, relaxor ferroelectric $BaTiO_3$-based ceramics are playing an important role in the area of energy density capacitors due to their low P_r, high P_{max} and low energy loss. In this work, a new relaxor ferroelectric $0.88BaTiO_3$–$0.12Bi(Li_{0.5}Nb_{0.5})O_3$ solid solution ceramic achieved a significantly enhanced dielectric breakdown strength (>270 kV cm^{-1}), discharge energy density (>2 J cm^{-3}) and charge–discharge efficiency (>88%). Moreover, good thermal stability in the wide range of 20–120 °C of the energy storage performance and a fast discharge speed ($\tau_{0.9} \leq$ 0.15 μs) were also observed.

Fig. 1a shows the XRD patterns of the 0.88BT–0.12BLN ceramics sintered at 1220 °C. From Fig. 1a, it is seen that the 0.88BT–0.12BLN ceramics exhibited a perovskite structure without any appreciable secondary impurity phases, indicating that BLN can diffuse into the BT lattices to form a solid solution in this composition. Based on Shannon's data, the equivalent ionic radius of Ba^{2+} (1.61 Å) in a 12 coordinate environment is larger than that of Bi^{3+} (1.11 Å) in the ABO_3 perovskite structure. The equivalent ionic radii of $(Li_{0.5}Nb_{0.5})^{3+}$ ions can be calculated by the following equation: $R = 0.5R(Li^+) + 0.5R(Nb^{5+}) = 0.70$ Å (ionic radii of Li^+ and Nb^{5+} are 0.76 Å and 0.64 Å, respectively).[29] The result shows that $(Li_{0.5}Nb_{0.5})^{3+}$ and Ti^{4+} have similar equivalent ionic radii. It is understandable that the $(Li_{0.5}Nb_{0.5})^{3+}$ ion can occupy the B sites. Moreover, Bi^{3+} is much larger than Ti^{4+} (0.605 Å). It is believed that Bi^{3+} ions and $(Li_{0.5}Nb_{0.5})^{3+}$ ions are more likely to enter the A-site and B-site in the BT–BLN ceramics, respectively. From the enlarged pattern of the (200) peak at about 45°, one can see that the crystal phase of 0.88BT–0.12BLN ceramics is a cubic phase. The cell parameter and

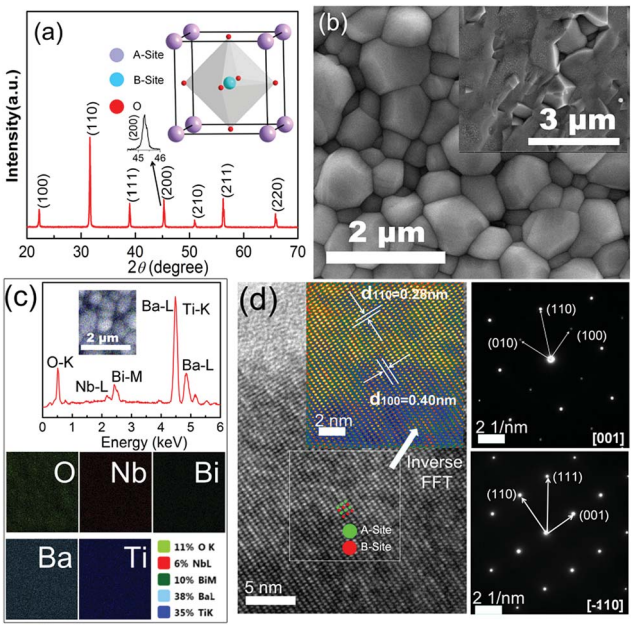

Fig. 1 (a) XRD patterns of the 0.88BT–0.12BLN ceramics; (b) SEM micrographs of the 0.88BT–0.12BLN ceramics; (c) EDX elemental mapping images of the 0.88BT–0.12BLN ceramics, green, O–K; red, Nb–L; olive, Bi–M; cyan, Ba–L; blue, Ti–K; the bright contrast corresponds to high density regions, suggesting compositional homogeneity related to the original surface; (d) the high-resolution TEM image, the inverse FFT(white square area) image, and the Selected Area Electron Diffraction (SAED) spots for the [0 0 1] and [−1 1 0] zone axes of 0.88BT–0.12BLN bulk ceramics, respectively.

volume values for 0.88BT–0.12BLN ceramics are calculated to be $a = 4.0178(9)$ Å and volume = 64.86 Å^3. Fig. 1b and c show SEM and elemental mapping of the 0.88BT–0.12BLN ceramics. As seen from Fig. 1b, the grain boundaries of 0.88BT–0.12BLN ceramics are clear and there is no obvious visible pore. The original surface and fractured surface micrographs indicate that the sintered 0.88BT–0.12BLN ceramics are quite dense and grain sizes are about 1 μm. Previous studies indicate that the dense microstructure and the small pore size in bulk ceramics can lead to high breakdown strength.[14] In order to confirm the composition of Ba, Ti, Bi, Nb, and O, elemental mapping analysis has been carried out at some selected positions of the 0.88BT–0.12BLN ceramics as shown in Fig. 1c. It can be seen that the Ba, Ti, Bi, Nb, and O elements are uniformly distributed in the 0.88BT–0.12BLN ceramics. Fig. 1d shows the high-resolution transmission electron microscopy (HR-TEM) image and selected area electron diffraction (SAED) pattern of the 0.88BT–0.12BLN bulk ceramics. The HR-TEM image clearly reveals a lattice fringe. Fig. 1d clearly displays an interplanar spacing of $d = 0.40$ nm and 0.28 nm, corresponding to the (100) and (110) crystal planes of 0.88BT–0.12BLN bulk ceramics. The SAED patterns of 0.88BT–0.12BLN bulk ceramics viewed along the [0 0 1] and [−1 1 0] zone axes are shown in Fig. 1d. The HR-TEM results also supported the XRD analysis.

Fig. 2a and b shows the temperature and frequency dependence of the dielectric constant (ε_r) and dielectric loss (tan δ) of the 0.88BT–0.12BLN ceramics. The $\varepsilon_r - T$ and tan $\delta - T$ curves

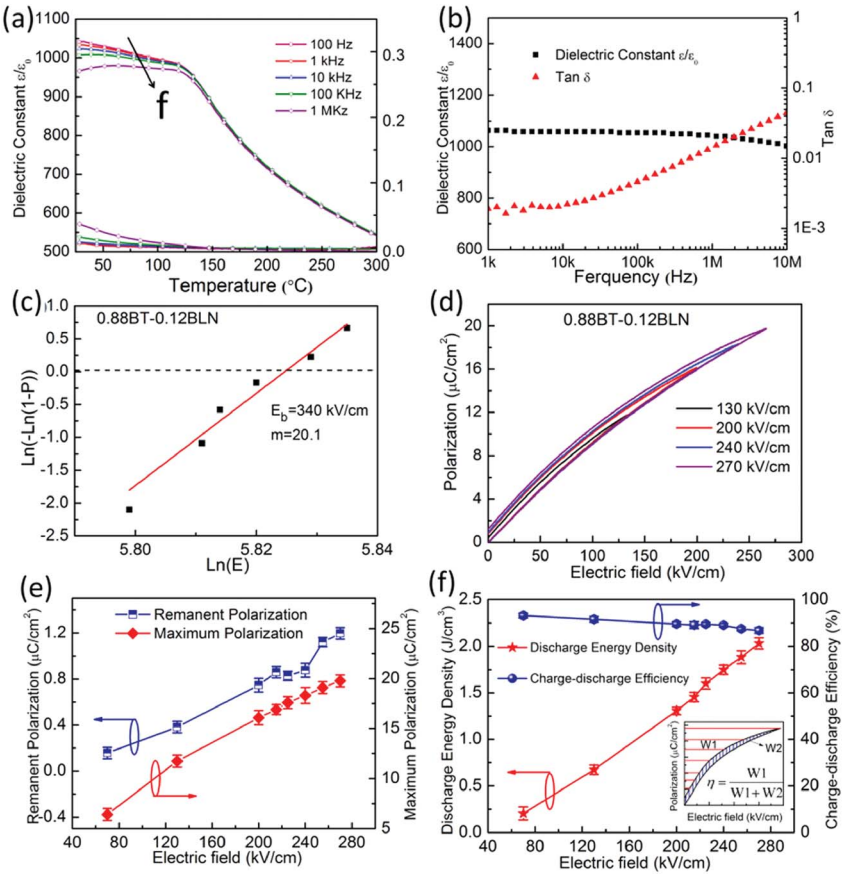

Fig. 2 (a) Temperature dependence of the dielectric constant and the loss of the 0.88BT–0.12BLN ceramics measured in the temperature range from 25 to 300 °C; (b) frequency dependence of the dielectric constant and the dielectric loss of 0.88BT–0.12BLN ceramics; (c) Weibull distributions and the fitting lines of the breakdown strength of 0.88BT–0.12BLN ceramics; (d–f) the unipolar P-E loops and the energy storage properties of 0.88BT–0.12BLN ceramics at different electric fields.

were measured at increasing frequencies from 100 Hz to 1 MHz. From Fig. 2a, it can be seen that the ε_r of the 0.88BT–0.12BLN ceramics exhibits good temperature stability (ε_r changes with temperature less than 10%) from 25 to 120 °C and then decreases as the temperature increases from 120 to 300 °C. The emergence of the relaxor behavior is caused by the addition of BLN to the BT ceramics. The tan δ decreases as the temperature increases from 25 to 300 °C and always maintains a low loss. Previous studies reported that $BiM_1M_2O_3$ can effectively mitigate the sintering temperature and dielectric losses.[24–26] From Fig. 2b, the ε_r becomes smaller as the frequency increases. Generally, it can be attributed to the dielectric relaxation in 0.88BT–0.12BLN ceramic. The tan δ exhibits a relatively low value of ~0.01 at a low frequency from 10^2 to 10^6 Hz, and a sharp increase appears above 10^7 Hz, which should be ascribed to the relaxor polarization loss. It indicates that BLN could mitigate dielectric losses significantly. The ε_r and tan δ values of the 0.88BT–0.12BLN ceramics vary slightly around 1180 and 0.01, respectively. The moderate dielectric permittivity (about 1000) is favorable for high breakdown strength. In order to obtain the value of intrinsic breakdown strength, the Weibull distribution of breakdown strength for 0.88BT–0.12BLN ceramics is shown in Fig. 2c. The Weibull distribution can be described by the following equations:[11,14]

$$X_i = \ln(E_i) \tag{4}$$

$$Y_i = \ln\left(-\ln\left(1 - \frac{i}{1+n}\right)\right) \tag{5}$$

where X_i and Y_i are the two parameters in the Weibull distribution function, E_i is the specific breakdown voltage of each specimen in the experiments, n is the sum of specimens of each sample, and i is the rank of specimens. From Fig. 2c, X_i and Y_i have a linear relationship and all data points fit well with the Weibull distribution and the shape parameter m is larger than 11 for each composition. According to the data given in Fig. 2c, the breakdown strength of 0.88BT–0.12BLN ceramics is 340 kV cm^{-1}. The values of breakdown strength are significantly higher than those of other BT-based bulk ceramics. Fig. 2d shows unipolar P–E loops of the 0.88BT–0.12BLN ceramics that are measured with 10 Hz triangular signals under different electric fields (Fig. S1†). As shown in Fig. 2d, the unipolar P–E loops become thick as the electric field increases. The P–E loops of 0.88BT–0.12BLN ceramics transform gradually from a saturated loop for pure BT ceramics into slim loops for 0.88BT–

Table 1 Comparison of the energy storage properties of 0.88BT–0.12BLN ceramics and BT-based ceramics

No.	Sample	E_b (kV cm^{-1})	W_{rec} (J cm^{-3})	η (%)	Ref.
1	$0.8BaTiO_3$–$0.2BiYO_3$	66	0.316	82.7	25
2	$0.91BaTiO_3$–$0.09BiYbO_3$	93	0.71	82.6	23
3	$0.90BaTiO_3$-$0.10BiInO_3$	140	0.753	89.4	25
4	$0.85BaTiO_3$–$0.15Bi(Zn_{2/3}Nb_{1/3})O_3$	131	0.79	93.5	24
5	$0.86BaTiO_3$–$0.14Bi(Zn_{1/2}Ti_{1/2})O_3$	120	0.81	94	26
6	$0.90BaTiO_3$–$0.10Bi(Mg_{2/3}Nb_{1/3})O_3$	143	1.13	93	27
7	$0.88BaTiO_3$–$0.12Bi(Mg_{1/2}Ti_{1/2})O_3$	224	1.81	88	28
8	$0.88BaTiO_3$–$0.12Bi(Li_{0.5}Nb_{0.5})O_3$	270	2.032	88	This work

0.12BLN ceramics (Fig. S2†). The results show that the ferroelectric properties of 0.88BT–0.12BLN ceramics are dramatically decreased with the BLN content. These observations indicate that BLN modification can destabilize the ferroelectric phase in BT ceramics. Fig. 2e shows P_r and P_{max} as a function of the electric field. With the electric field increasing from 40 to 270 kV cm^{-1}, the P_r and P_{max} values increase from 0.15 and 6.42 μC cm^{-2} to 1.19 and 19.77 μC cm^{-2}, respectively. The 0.88BT–0.12BLN relaxor ceramic is more likely to be used for high W_{dis} because of the small P_r. Fig. 2f represents the discharge energy density and charge–discharge energy efficiency of 0.88BT–0.12BLN as a function of the electric field. It can be observed that discharge energy density increases while charge–discharge energy efficiency decreases as the electric field increases. In Fig. 2f, the discharge energy density of 0.88BT–0.12BLN increases from 0.21 to 2.032 J cm^{-3} with the increase of the electrical field from 40 to 270 kV cm^{-1}. The charge–discharge energy efficiency is determined by the ratio of the discharge energy density and charge energy density. With the increases of the applied electric field, the charge–discharge energy efficiency decreases because of the increases of energy loss density. For the energy storage efficiency, it always keeps a high efficiency (>88%) when the applied electric field reaches 270 kV cm^{-1}. The 0.88BT–0.12BLN ceramics exhibit optimum energy storage properties with a charge energy density of 2.34 J cm^{-3}, a discharge energy density of 2.032 J cm^{-3} and a charge–discharge efficiency of ~88% under 270 kV cm^{-1}. In this work, the breakdown strength and discharge energy density values are considerably higher than those of some other lead-free ceramics, indicating that the 0.88BT–0.12BLN ceramics are a promising candidate for high power energy storage applications. Table 1 compares the discharge energy density and electric field performance of our samples with other promising candidate materials reported previously. The large discharge energy density (2.032 J cm^{-3}) of 0.88BT–0.12BLN ceramics is almost 1.5 times higher than those of other lead-free bulk ceramics. Furthermore, a high breakdown strength (>270 kV cm^{-1}) and high energy efficiency (>88%) are concomitantly achieved in the 0.88BT–0.12BLN, which makes it outstanding as an environmentally friendly material for electrostatic energy storage.

Fig. 3 shows P_r, P_{max} and the energy storage properties of 0.88BT–0.12BLN ceramics as a function of temperature from 20 to 120 °C under 150 kV cm^{-1}. Fig. S3† shows the *P*–*E* loops of 0.88BT–0.12BLN ceramics at various temperatures from 20 to 120 °C under 150 kV cm^{-1}. As is well known, the capacitors exhibit a heat phenomenon in the application. Therefore, thermal stability is regarded as one pivotal factor for electronic materials. So it is important to study the thermal stability of the 0.88BT–0.12BLN ceramics. Fig. 3a indicates that the P_r and P_{max} values decreased from 1.24 to 0.8 μC cm^{-2} and from 13.49 to 11 μC cm^{-2}, respectively, when the temperature increases from 20 to 120 °C. It can be seen that ε_r also decreases slightly with a temperature increase from 20 to 120 °C in Fig. 2a. This relaxor behavior is caused by the addition of BLN in the BT ceramics. The polarization response of the 0.88BT–0.12BLN ceramics exhibits good temperature stability from 20 to 120 °C because of the relaxor behavior. Fig. 3b shows the discharge energy density and the charge–discharge energy efficiency exhibit a good thermal stability from 20 to 120 °C. The discharge energy density and charge–discharge energy efficiency vary slightly from 0.9 to 0.8 J cm^{-3} and around 84%, respectively, when the

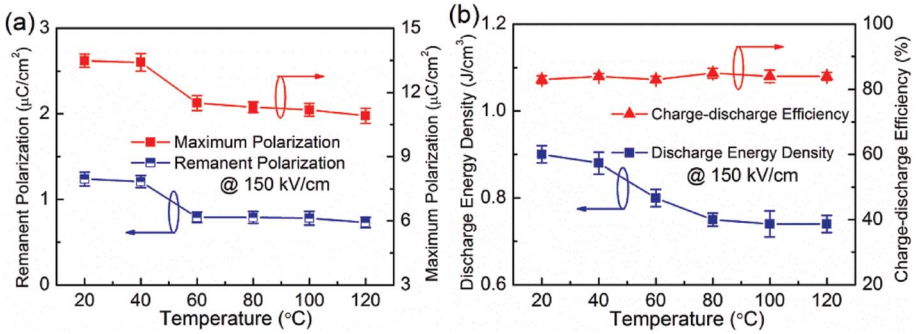

Fig. 3 The P_r, P_{max} and energy storage properties of 0.88BT–0.12BLN ceramics at different temperatures under 150 kV cm^{-1}.

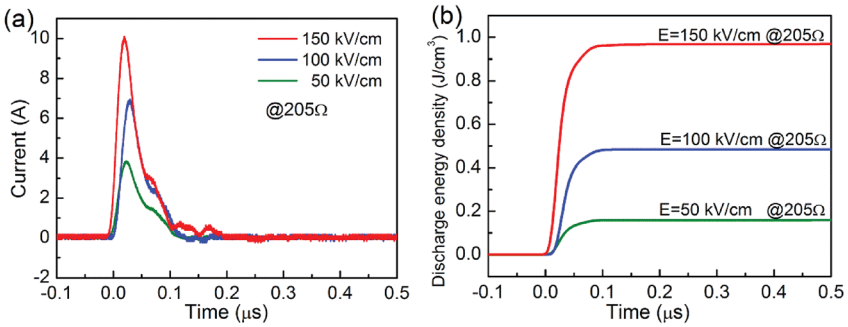

Fig. 4 Pulsed discharge current (a) and time dependence of the discharge energy density (b) of 0.88BT–0.12BLN ceramics under different electric fields.

temperature increases from 20 to 120 °C. These results suggest that 0.88BT–0.12BLN ceramics have excellent thermal stability of the energy storage capability.

Fig. 4 shows the discharging speed behavior of 0.88BT–0.12BLN ceramics under different electric fields. A fast discharge time is required for the high energy density capacitors. The discharge speed and discharge energy density are measured using a high-speed capacitor discharge circuit (RC circuit). In this circuit, the discharge energy is measured using a load resistor (R_L) in series with the 0.88BT–0.12BLN ceramic samples (Fig. S4†). The samples are charged to 50, 100, 1 and 50 kV cm^{-1} followed by discharge across a 205 Ω load. The discharge energy density can be calculated as:[30,31]

$$W = R\int i^2(t)\mathrm{d}t/V \quad (6)$$

where $i(t)$ is the discharge current detected by using the oscillograph, R is the total load resistance (205 Ω), and V denotes the volume of the measured sample. The experimental discharge time $\tau_{0.9}$ is defined as the time for the discharge energy in the load to achieve 90% of the final value from the discharge profiles.[18] Fig. 4a shows the dependence of discharge current waveforms on discharge time under different electric fields. It indicates that all the discharge processes last about 0.50 μs. The discharge energy density as a function of discharge time under different electric fields is shown in Fig. 4b. The $\tau_{0.9}$ of all samples is less than 0.15 μs. That means 90% of the discharge energy density can be released in about 0.15 μs. It indicates that 0.88BT–0.12BLN ceramics are very promising for pulsed power capacitors.

Conclusions

In summary, this work demonstrates significantly enhanced breakdown strength and improved discharge energy density of BT-based ceramics through incorporation of BLN forming a perovskite solid solution. High breakdown strength and discharge energy density were obtained in the 0.88$BaTiO_3$–0.12$Bi(Li_{0.5}Nb_{0.5})O_3$ (0.88BT–0.12BLN) ceramics prepared by using a conventional solid state reaction method. XRD and SAED analysis indicated that 0.88BT–0.12BLN exhibited a perovskite structure. The 0.88BT–0.12BLN ceramics exhibited good energy storage properties with high dielectric breakdown strength (>270 kV cm^{-1}), discharge energy density (>2 J cm^{-3}) and charge–discharge efficiency (>88%). The great thermal stability in the wide range of 20–120 °C of the energy storage performance and a fast discharge speed ($\tau_{0.9} \leq 0.15$ μs) were also observed. All the results indicate that the 0.88$BaTiO_3$–0.12$Bi(Li_{0.5}Nb_{0.5})O_3$ ceramic is a promising lead-free material for high density energy storage capacitor application.

Conflicts of interest

There are no conflicts of interest to declare.

Acknowledgements

This work was supported by the National Natural Science Foundation of China (U1632146), the Young Star Project of Science and Technology of Shaanxi Province (2016KJXX-34), the Fundamental Research Funds for the Central University, and the 111 Project of China (B14040). The SEM and TEM work was done at the International Center for Dielectric Research (ICDR), Xi'an Jiaotong University, Xi'an, China and the authors thank Ms. Yan-Zhu Dai and Mr Chuan-Sheng Ma for their help in using SEM and TEM.

References

1 G. R. Love, *J. Am. Ceram. Soc.*, 1990, **73**, 323–328.
2 I. Burn and D. M. Smyth, *J. Mater. Sci.*, 1972, **7**, 339–343.
3 J. J. Xu, Z. L. Wang, D. Xu, F. Z. Meng and X. B. Zhang, *Energy Environ. Sci.*, 2014, **7**, 2213–2219.
4 Z. C. Shi, R. H. Fan, Z. D. Zhang, L. Qian, M. Gao, M. Zhang, L. T. Zheng, X. H. Zhang and L. W. Yin, *Adv. Mater.*, 2012, **24**, 2349–2352.
5 W. B. Hu, Y. Liu, R. L. Withers, T. J. Frankcombe, L. Norén, A. Snashall, M. Kitchin, P. Smith, B. Gong, H. Chen, J. Schiemer, F. Brink and J. W. Leung, *Nat. Mater.*, 2013, **12**, 821–826.
6 Q. Li, G. Zhang, F. Liu, K. Han, M. R. Gadinski, C. Xiong and Q. Wang, *Energy Environ. Sci.*, 2015, **8**, 922–931.
7 M. K. Han, X. W. Yin, L. Kong, M. Li, W. Y. Duan, L. T. Zhang and L. F. Cheng, *J. Mater. Chem. A*, 2014, **2**, 16403–16409.

8 W. P. Li, L. Jiang, X. Zhang, Y. Shen and C. W. Nan, *J. Mater. Chem. A*, 2014, **2**, 15803–15807.
9 X. F. Su, B. C. Riggs, M. Tomozawa, J. K. Nelsonc and D. B. Chrisey, *J. Mater. Chem. A*, 2014, **2**, 18087–18096.
10 T. Q. Shao, H. L. Du, H. Ma, S. B. Qu, J. Wang, J. F. Wang, X. Y. Wei and Z. Xu, *J. Mater. Chem. A*, 2017, **5**, 554–563.
11 Y. F. Wang, J. Cui, L. X. Wang, Q. B. Yuan, Y. J. Niu, J. Chen, Q. Wang and H. Wang, *J. Mater. Chem. A*, 2017, **5**, 4710–4718.
12 D. P. Shay, N. J. Podraza, N. J. Donnelly and C. A. Randall, *J. Am. Ceram. Soc.*, 2012, **95**, 1348–1355.
13 J. J. Zhang, L. D. Ji, X. R. Jia, J. Y. Wang, J. W. Zhai and Y. Zhou, *J. Am. Ceram. Soc.*, 2015, **98**, 97–103.
14 W. B. Li, D. Zhou and L. X. Pang, *Appl. Phys. Lett.*, 2017, **110**, 132902.
15 Z. C. Shi, R. H. Fan, K. L. Yan, K. Sun, M. Zhang, C. G. Wang, X. F. liu and X. H. Zhang, *Adv. Funct. Mater.*, 2013, **23**, 4123–4132.
16 X. L. Li, X. W. Yin, M. K. Han, C. Q. Song, X. N. Sun, H. L. Xu, L. F. Cheng and L. T. Zhang, *J. Mater. Chem. C*, 2017, **5**, 7621–7628.
17 B. Y. Qu, H. L. Du and Z. T. Yang, *J. Mater. Chem. C*, 2016, **4**, 1795–1803.
18 H. R. Jo and C. S. Lynch, *J. Appl. Phys.*, 2016, **119**, 024104.
19 Q. F. Zhang, H. F. Tong, J. Chen, Y. M. Lu, T. Q. Yang, X. Yao and Y. B. He, *Appl. Phys. Lett.*, 2016, **105**, 262901.
20 B. B. Liu, X. H. Wang, Q. C. Zhao and L. T. Li, *J. Am. Ceram. Soc.*, 2015, **98**, 2641–2646.
21 Y. H. Huang, Y. J. Wu, W. J. Qiu, J. Li and X. M. Chen, *J. Eur. Ceram. Soc.*, 2015, **35**, 1469–1476.
22 L. Zhou, P. M. Vilarinho and J. L. Baptista, *J. Eur. Ceram. Soc.*, 1999, **19**, 2015–2020.
23 Z. B. Shen, X. H. Wang, B. C. Luo and L. T. Li, *J. Mater. Chem. A*, 2015, **3**, 18146–18153.
24 L. W. Wu, X. H. Wang and L. T. Li, *RSC Adv.*, 2016, **6**, 14273–14282.
25 M. Wei, J. H. Zhang, K. T. Wu, H. W. Chen and C. R. Yang, *Ceram. Int.*, 2017, **43**, 9593–9599.
26 X. B. Zhao, Z. Y. Zhou, R. H. Liang, F. H. Liu and X. L. Dong, *Ceram. Int.*, 2017, **43**, 9060–9066.
27 T. Wang, L. Jin, C. C. Li, Q. Y. Hu and X. Y. Wei, *J. Am. Ceram. Soc.*, 2015, **98**, 559–566.
28 Q. Y. Hu, L. Jin, T. Wang, C. C. Li, Z. Xing and X. Y. Wei, *J. Alloys Compd.*, 2015, **640**, 416–420.
29 R. D. Shannon, *J. Appl. Phys.*, 1993, **73**, 348–366.
30 R. Xu, Z. Xu, Y. J. Feng, X. Y. Wei, J. J. Tian and D. Huang, *J. Appl. Phys.*, 2016, **119**, 224103.
31 R. Xu, Z. Xu, Y. J. Feng, X. Y. Wei, J. J. Tian and D. Huang, *Appl. Phys. Lett.*, 2016, **109**, 032903.

